Desalination and Water Treatment
www.deswater.com
1944-3994/1944-3986 © 2012 Desalination Publications. All rights reserved
doi: 10.1080/19443994.2012.672174

43 (2012) 212–220
April

Taylor & Francis
Taylor & Francis Group

Time-series image analysis for investigating SWRO fouling mechanism

Moonkhum Monruedee[a], Sarper Sarp[b], Young Geun Lee[c], Joon Ha Kim[a,b,*]

[a]*School of Environmental Science and Engineering, Gwangju Institute of Science and Technology (GIST), 261 Cheomdan-gwagiro, Buk-gu, Gwangju 500-712, Korea*
Tel. +82 62 970 3277; Fax: +82 62 970 2434; email: joonkim@gist.ac.kr
[b]*Sustainable Water Resource Technology Center, Gwangju Institute of Science and Technology (GIST) 261 Cheomdan-gwagiro, Buk-gu, Gwangju 500-712, Korea*
[c]*Water Business Group, Doosan Heavy Industries & Construction Co., Ltd., Gyeongsangnam-do 642-792, Korea*

Received 25 December 2011; Accepted 10 February 2012

ABSTRACT

The fouling behavior of seawater reverse osmosis membranes has yet to be definitively investigated due to the complexity of seawater compositions. In this study, a time-series image analysis (TSIA) was performed to investigate the fouling mechanism using scanning electron microscopy (SEM) and atomic force microscopy (AFM). The fouling experiments were conducted with synthetic seawater (SS) and SS mixed with humic acid substances (SHA). The effect of operational time was investigated for 2, 4, 6, 8, 12, and 20 h. According to the TSIA results, different fouling characteristics between SS and SHA experiments were observed. In the SS case, the fouling mechanism is the interaction between inorganic particles and the membrane surface as well as interaction between inorganic particles and the deposited foulants. Then, increased accumulation of deposited foulants was observed with respect to the operational time. However, in the presence of humic acid, the fouling mechanism was significantly influenced by the adsorption of humic acid onto the membrane surface at the initial stage (first 2 h). This organic layer traps inorganic particles and organic substances, and accelerates the fouling formation on the membrane surface, thereby leading to a greater flux decline compared to the SS experiment.

Keywords: Fouling mechanism; Image analysis; Membrane morphology; Reverse osmosis; Surface roughness

1. Introduction

Insufficient water supplies in areas around the world have led to an increased interest in freshwater production via a diverse range of processes. In particular, one promising solution for overcoming the expected water shortage is desalination technology [1]. In recent years, seawater reverse osmosis (SWRO) desalination has become the leading global technology for seawater desalination, because it shows higher economical efficiency compared with multistage flash and multi-effect distillation [2–4]. Furthermore, recent research relating to SWRO processes has focused on energy saving and the cost reduction [5–8]; as such, it is expected that SWRO desalination technology will become more popular and be able to produce freshwater with less energy consumption.

*Corresponding author.

However, membrane fouling remains as a major problem limiting the performance and increasing the cost of desalination processes [9–12]. The main foulants in the SWRO process are inorganic compounds, colloidal or particulate matter, dissolved organic substances, and micro-organisms [13,14]. Numerous research groups have studied the SWRO fouling mechanism, though membrane fouling is yet to be fully characterized—primarily due to the inherent complexity of seawater. Seawater is composed of 40,000–50,000 mg/L of inorganic compounds, whereas it only contains 2–5 mg/L of organic compounds [10]. Interestingly, however, it has been reported that organic compounds cause more acute problems in the filtration process than inorganic compounds [10]. Among the organic compounds in seawater, 80–90% are represented by humic acid substances. Humic acid substances cause fouling via organic adsorption and can also be a substrate for micro-organisms, leading to irreversible fouling [15].

To date, significant efforts have been dedicated to investigate the mechanisms and control methods of RO fouling caused by organic compounds [16–18]. In practical terms, a decrease in the permeate flux and an increase in the operating pressure are commonly used to diagnose the degree of membrane fouling [19,20]. In addition, a number of foulant characterization and autopsy techniques have been applied in attempts to obtain a more comprehensive understanding of the membrane, including the surface structure and morphology, foulant composition analysis, surface potential, surface hydrophobicity/hydrophilicity, and the identification of surface functional groups [21,22]. However, the previous studies have only illustrated fouling development by comparing clean and fouled membranes, which cannot fully explain the fouling formation with respect to time and mechanism of fouling [23]. In order to overcome these limitations, time-series fouling experiments (TSFEs) were selected here as a means to investigate the formation of fouling during SWRO process. Time-series data provide unique information for each operating time-period, which leads to a better understanding of the fouling mechanism during SWRO processes [24]. In this study, both TSFEs in addition to scanning electron microscopy (SEM) and atomic force microscopy (AFM) membrane morphology analyses were used. Thus, we posit that TSFEs coupled with image analyses can be used to effectively describe the fouling mechanism of humic acid during the SWRO process.

2. Materials and methods

2.1. Reverse osmosis membrane

One commercial RO membrane (RE8040-SHN400, Woongjin Chemical Co., Ltd., Korea) was used for all fouling experiments; the RO membrane was polyamide thin-film composite (TFC). Membrane coupons were kept in deionized (DI) water at 4°C at all times, and the DI water was replaced at regular intervals.

2.2. Feed solution

Two feed solutions were used: synthetic seawater (SS) and SS mixed with a humic acid compound (SHA). The SS was prepared by dissolving commercially available sea salts (Sigma-Aldrich, USA) into DI water to a concentration of 35 g/L, which was then filtered through a Whatman 0.45 m filter (Advantec MFS, Inc., USA). SHA was prepared by adding humic acid (HA) stock solution (Sigma-Aldrich, USA) into SS. The HA stock solution was prepared (2 g/L) by dissolving HA in DI water and mixing for over 24 h to ensure complete dissolution. The stock solution was then stored in a sterilized glass bottle at 4°C. Subsequently, this stock solution was mixed (5 mg/L) into SS before performing the SHA fouling experiment. The concentration of humic acid was fixed at 5 mg/L because it represented the average concentration of humic acid in seawater. The pH of feed solutions was adjusted to 7.0 ± 0.1 by addition of 0.1 M NaOH or HCl as needed. The feed solution compositions are shown in Table 1.

2.3. Crossflow membrane filtration test unit

TSFEs were performed with a lab-scale crossflow membrane filtration (CMF) test unit (SEPA CF, Osmonics, Inc., USA). The total effective area of the membrane was 140 cm^2, and a 0.1194 cm (47 mil) feed spacer was placed on the feed side to both distribute the feed flow as well as protect the membrane from high pressure [25]. Both permeate and retentate were

Table 1
Composition of feed solution

Components (mg/L)	Sea salts[a]	SS[b]	SHA[b]
Chloride (Cl^-)	19,290	17,582	17,483
Sodium (Na^+)	10,780	8,855	9,117
Sulfate (SO_4^{2-})	2,660	2,422	2,651
Magnesium (Mg^{2+})	1,320	1,246	1,261
Potassium (K^+)	420	419	420
Calcium (Ca^{2+})	400	380	391
Strontium (Sr^{2+})	8.8	8.8	8.1
Carbonate (bicarbonate, HCO_3^-)	200	–[c]	–[c]

[a]Concentration based on specification sheet of sea salts.
[b]Results obtained by ion chromatography.
[c]Concentration of carbonate in feed solutions (did not analyze).

recirculated back to the feed reservoir. In addition, a chiller/heater with a stainless steel coil was used to maintain a constant temperature in the feed solution.

2.4. Time-series fouling experiments

Experiments were performed at a constant flow rate (0.5 L/min), pressure (55 bar), and temperature (25°C). All experiments were conducted in a recycle mode. The TSFEs were then sequentially processed as follows. First, the membrane was compacted and stabilized with DI water for 12 h. After reaching a steady state, DI water was replaced with SS for the SS fouling experiments (SSEs); SHA fouling experiments (SHAEs) were also carried out using this methodology. Both SSE and SHAE were carried out at operating time durations of 2, 4, 6, 8, 12, and 20 h. At the end of each experiment, the fouled membranes were preserved in an airtight container at 4°C prior to further image analysis.

Since the membrane surface is structurally a heterogeneous material, flux decline behaviors can be different when batch experiments are performed [26]. In order to ensure that all TSFEs were performed under almost identical conditions, six experiments during the operating time of 20 h, feed flow rate of 0.5 L/min, pressure of 55 bar, and temperature of 25°C were run with both solutions. Then, the standard deviation range of water flux decline of TSFEs was obtained. Only fouled membranes from experiments in this standard deviation range were used for further imaging analyses.

2.5. Image analysis of time-series fouled membranes

In order to characterize the fouling on the membrane surface, both SEM/EDX and AFM were performed. SEM/EDX (S-4700, Hitachi, Japan) was used to examine the topography of the membrane surface and the composition of the top layer of fouling. Collected membranes were dried before being coated with 3–4 nm of platinum using an Ion Sputter E-1030 (Hitachi, Japan); the coated membranes were then scanned with SEM. AFM imaging (X-100 AFM, Park Systems, Korea) was used to visualize membrane surface morphology. AFM was performed in non-contact mode with a scan area of 50×50 μm. Next, the average roughness (Ra) of the membrane surface was calculated using the Scanning Probe Image Processor (SPIP) image processing and analysis program (SPIP software, Image Metrology A/S, Denmark). The values of averages and standard deviations of the elemental analysis and roughness were obtained by scanning each fouled membrane 36 times from the different positions. The overall experimental design for the TSFEs is shown in Table 2.

3. Results and discussion

3.1. Time-series fouling experiments

Fig. 1 shows the permeate flux decline with respect to the operational times for all TSFEs. The gray areas represent the standard deviations range of TSFEs, which were obtained from six experiments as mentioned before. At the end of the each fouling test, the permeate flux of SSE and SHAE decreased by 18 and 26%, respectively. In both cases, the permeate flux decline showed a rapid initial increase, then a more gradual increase until the end of the fouling test. However, it was found that the fouling mechanisms of SSE and SHAE were different. Initially, fouling mechanism of SSE was based on the interaction between the inorganic foulant and the membrane surface [27]. Then, the accumulation of particles on membrane surface was observed. On the other hand,

Table 2
Experimental design for TSFEs

Experiment and analysis	Experiments[a]	TSFEs[b]	Image analysis[c]	
			SEM	AFM
Number of repetitions	Six	One (per each operational time)	36	36
Obtained results	• Standard deviation range for TSFE	• Permeate flux	• 2D time-series images of fouled membrane	• 3D time-series images of fouled membrane
		• Time-series fouled membranes	• Elemental composition	• Roughness values

[a]All experiments were carried out at an operating time of 20 h.
[b]Each TSFE was performed at operating times of 2, 4, 6, 8, 12, and 20 h.
[c]The best image was selected as a representative of each operating time among 36 samples.

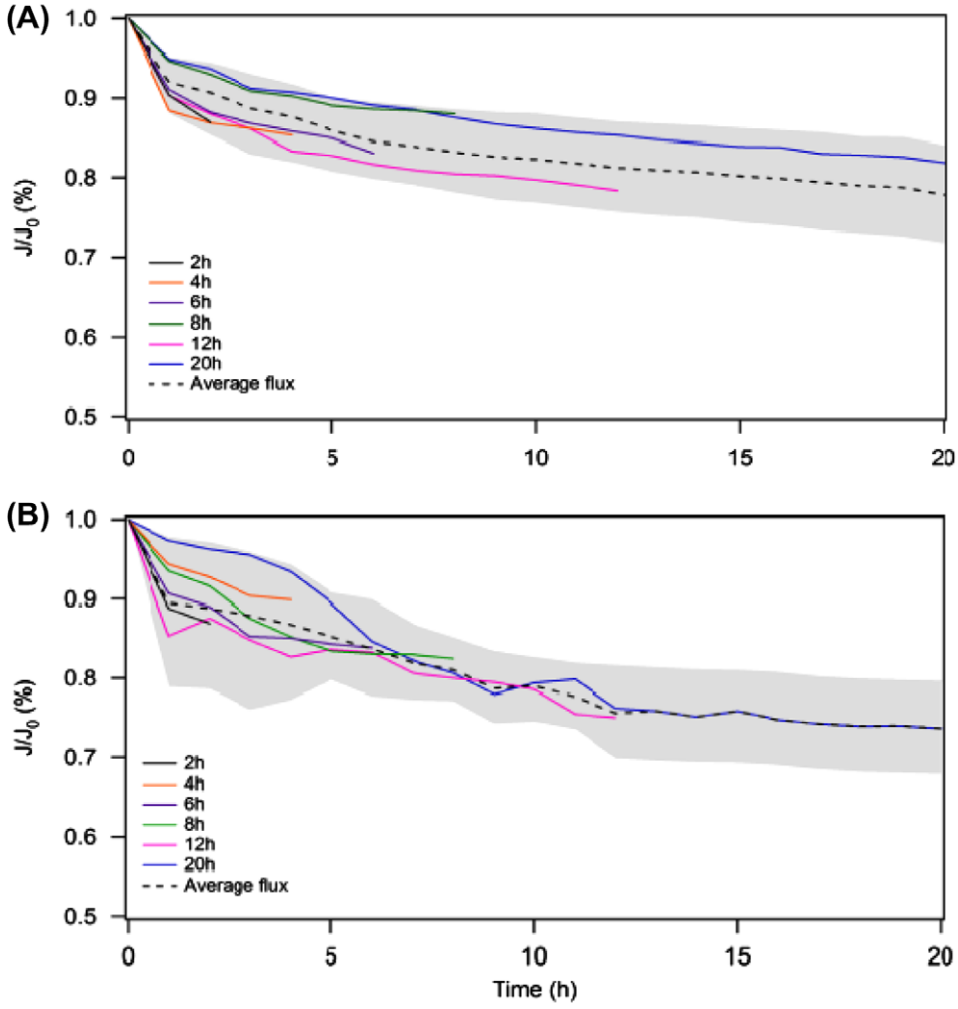

Fig. 1. Permeate flux decline of SSE (A) and SHAE (B) vs. operational time. Gray areas indicate the standard deviation range and black dotted lines denote the average permeate flux of six experiments of 20 h each. Colored lines show the flux decline of fouling tests at operating time of 2, 4, 6, 8, 12, and 20 h.

with SHAE it is highly possible that the fouling formation was influenced by the adsorption of organic substances during the first 2 h. This sudden formation of an organic layer resulted in a high initial flux decline. Therefore, the formation of fouling can be initially explained by both the adsorption of organic substances as well as the deposition of inorganic particles onto the membrane surface. Then, fouling formation continued due to the interaction between inorganic particles and the existing organic layer [28].

3.2. Time-series image analysis using AFM

Fig. 2 shows the surfaces of the fouled membranes obtained using AFM. AFM image of clean membrane showed that membrane surface of RO membrane is not completely flat and smooth. Thus, foulants tended to accumulate in the valleys on the membrane surface causing valley clogging and flux decline during the filtration process. The results show that fouled membranes had different morphologies from the clean membrane; the effect of operational time on fouling formation can also be clearly seen. The figure indicates that the fouling mechanisms of SSE and SHAE were different. AFM images of SSE showed that fouling layer gradually formed by the sparse deposition of inorganic particles on the membrane surface at the beginning stage of filtration. Then, more particles subsequently and continuously accumulated on the fouled membrane surface. In contrast, the surfaces of the fouled membrane from SHAE were fully covered by an organic layer and some inorganic particles at an earlier stage. Later, the fouling was formed by both the adsorption of organic compounds and the deposition of inorganic particles onto the existing organic layer. Based on these results, it is posited here that humic

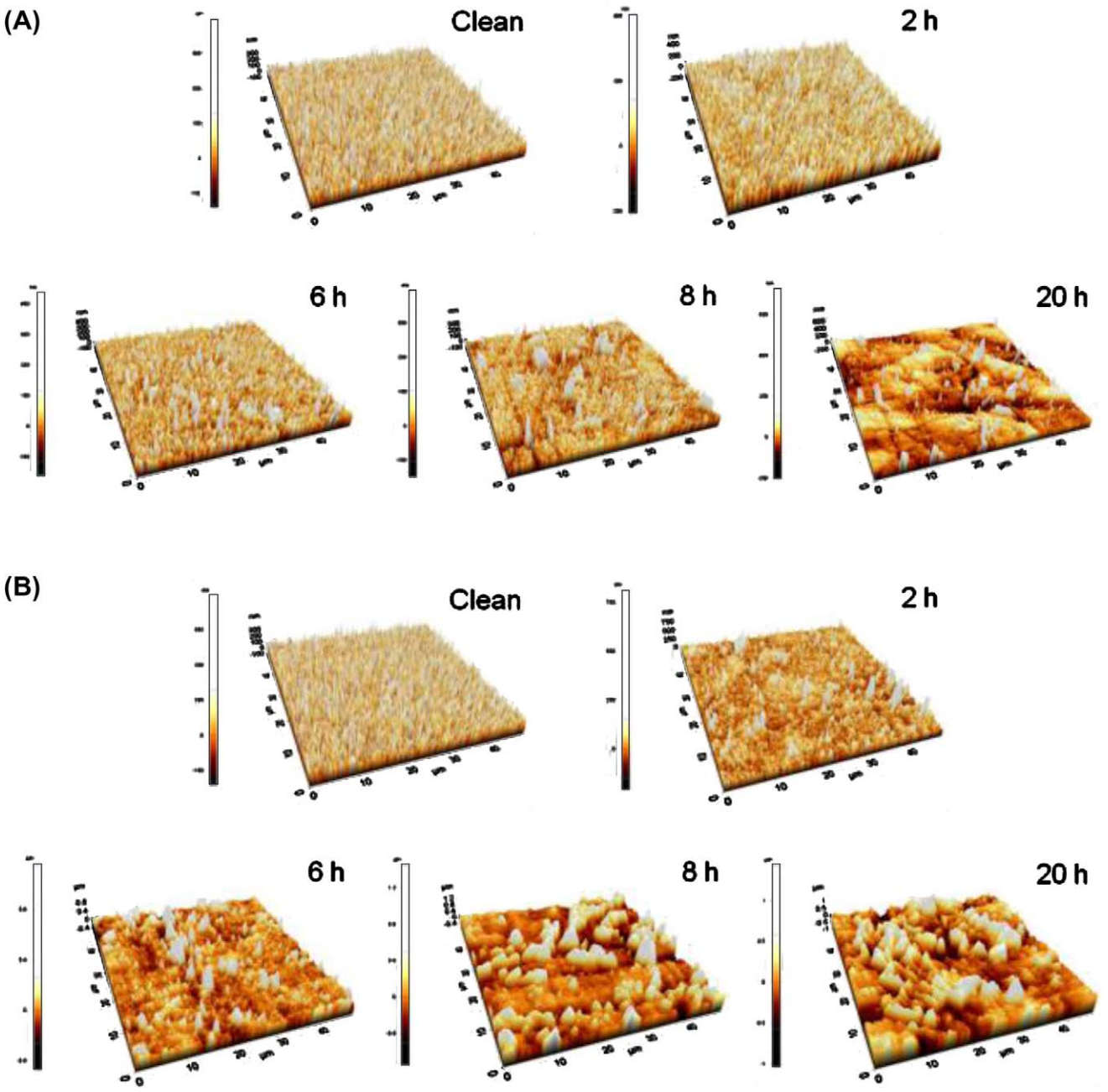

Fig. 2. Time-series AFM images of SSE (A) and SHAE (B) at different operating times (i.e. 2, 4, 6, 8, 12, 20 h). The dimensions of both X and Y are 50 μm.

compounds formed a layer similar to a cake layer on the membrane surface and accelerated the fouling formation [29].

In addition, the difference in membrane surface morphology can be explained by the Ra and root mean square roughness (RMS) (Table 3). The Ra and RMS of fouled membrane of SSE had increasing trend when the operational time increased due to the accumulation of inorganic particles. The Ra and RMS of SHAE at 20 h of filtration were relatively lower to those of SSE. Moreover, its roughness values slowly increased after initiation of the filtration process and then suddenly decreased at 8 h—which may be due to instability of the organic layer. Thus, it can be concluded that the surface of the fouled membrane obtained from SHAE becomes smoother than the one obtained from SSE after 20 h of filtration process due to the organic layer.

Table 3
Roughness measurement on RO fouled membrane at different operational times

Operational time	RMS (μm)		Ra (μm)	
	SSE	SHAE	SSE	SHAE
0	69.00 ± 2.4	69.00 ± 2.4	54.50 ± 1.9	54.50 ± 1.9
2	87.77 ± 8.3	111.05 ± 9.3	70.38 ± 8.2	79.01 ± 8.2
4	91.85 ± 5.9	120.52 ± 9.1	69.11 ± 2.3	83.13 ± 4.0
6	96.88 ± 6.7	123.88 ± 8.9	74.36 ± 6.3	91.47 ± 5.6
8	122.54 ± 9.0	96.31 ± 7.5	98.26 ± 8.5	73.38 ± 5.4
12	150.4 ± 4.5	99.58 ± 8.2	119.31 ± 8.8	71.54 ± 9.1
20	145.47 ± 7.0	110.58 ± 7.0	108.34 ± 3.5	81.60 ± 8.2

RMS: root mean square roughness; Ra: average roughness.

Results of the SEM image analysis were similar to those obtained in the AFM image analysis. Fouling formation started by the initial accumulation of foulants onto membrane surface and then followed by the extension of the initial deposition. In Fig. 3, for both cases, the different morphologies of the membrane surfaces could be visualized. The surface of fouled membranes from SSE shows that inorganic particles begin depositing onto the membrane surface before they begin to accumulate appearing in the greater number until the end of filtration process, while membrane surface is still observable after 20 h of filtration. However, fouled membranes obtained from SHAE were significantly affected by organic fouling. Therefore, the non-pattern formation of inorganic particles fixed in the organic layer can only be observed in SHAE.

Interestingly, the high-resolution SEM images of fouled membranes obtained after 2 h of operational time revealed the effect of humic substances on SWRO fouling (Fig. 4). The membrane surface of SHAE was completely covered with an organic layer, whereas the membrane surface of SSE was still visible. Therefore, the SHAE membrane surface has more potential to interact with inorganic particles to form a thick fouling layer, which significantly increases the resistance to permeate flow (Fig. 1).

3.3. Characterization of foulant compositions

The chemical compositions of the surfaces of the fouled membranes were analyzed to elucidate their behavior with respect to fouling formation. Table 4 shows the relative percentages of deposited elements for SSE and SHAE with respect to the operating time. The values for 0 h indicate the preliminary compositions of the clean membrane; an elemental analysis using SEM/EDX showed that surface of the clean membrane consists of carbon (C), oxygen (O), and sulfur at 83.04, 14.85, and 1.14%, respectively.

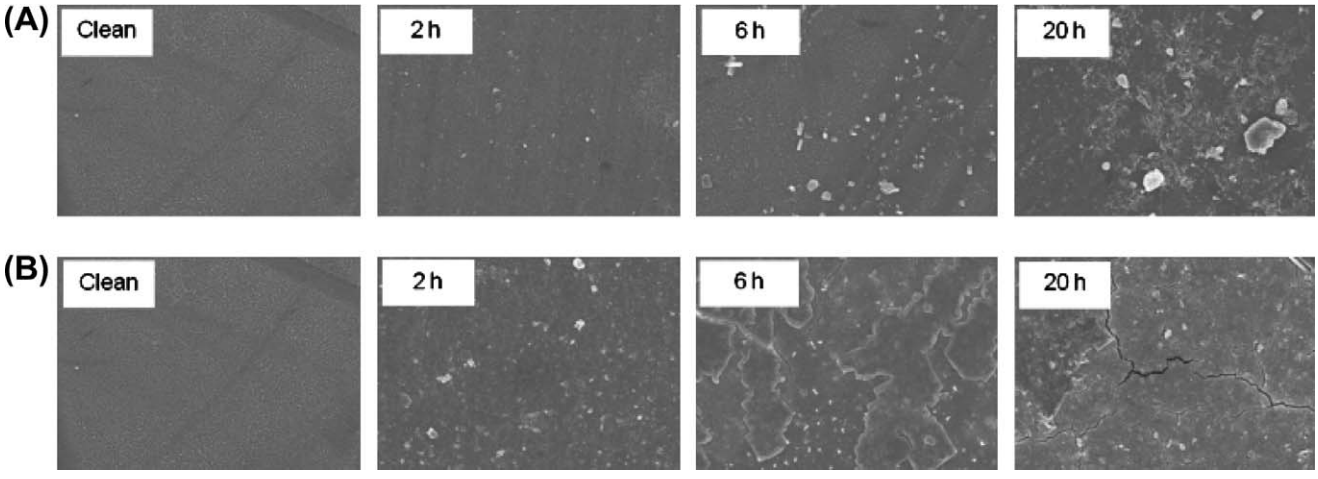

Fig. 3. SEM time-series images: (A) SEM images of SSE and (B) SEM images of SHAE. The image scanning of (A) and (B) was operated at a distance of 20 μm and magnification of 20,000×.

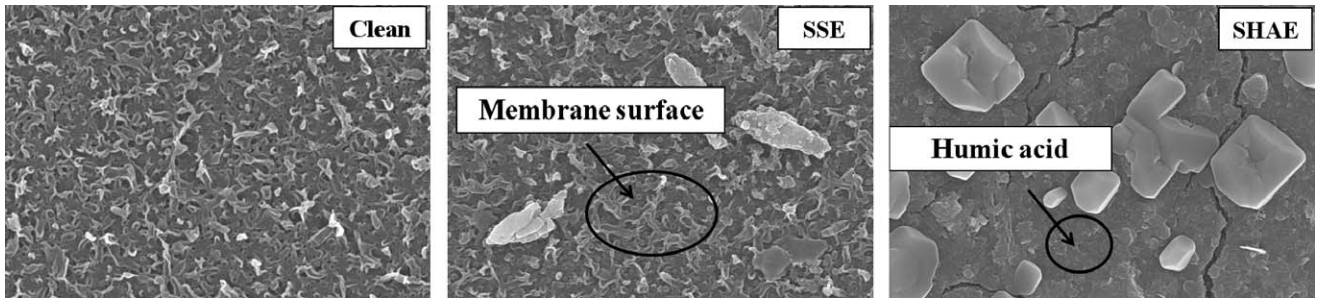

Fig. 4. High-resolution SEM images of clean membrane (left), fouled SSE membrane (middle), and fouled SHAE membrane (right) at operating time duration of 2 h. The image scanning was operated at a distance of 3 μm and magnification of 15,000×.

3.3.1. Carbon

According to Table 4, C is a major component of the clean membrane surface, the relative percentage of C was high at the initial stage. However, as the membrane surface became covered by foulants for 4 h, the percentage of C gradually decreased. Then, the percentage of C increased suddenly at 6 h for both cases, which might be a result of the decrease in O percentage. Then, C continued to decrease with operational time until the end of the fouling tests. At the end of the fouling test period, the percentage of C for SSE and SHAE membranes decreased from 83.04 to 69.44% and from 83.04 to 75.84%, respectively. The higher percentage of C in SHAE was due to the accumulation of organic substances on the membrane surface.

3.3.2. Oxygen

The percentage of O in the top layer of fouling increased as a function of time for both cases. In SSE and SHAE, O increased from an initial value of 14.85% to 23.61 and 28.78%, respectively. The increase of O on the fouled SSE membrane surface was the result of an inorganic O source as no organic foulant was mixed in the feed solution. According to Table 1, the concentrations of Ca, Mg, and SO_4^{2-} in feed water are not high compared to the concentration of Na. Therefore, it can be assumed that the enhanced percentage of O either originates from free carbonate or $NaHCO_3$, rather than from $CaCO_3$, $CaSO_4$, $MgSO_4$, or other inorganic foulants; the compositions of Ca, S, and Mg on the surfaces of the fouled membranes were relativly low. In SHAE, it is shown that the final percentage of O was higher than SSE because the feed solution of SHAE consists of organic compounds that contain more O and also it is possible that the presence of organic layer played an important role in trapping more oxides onto membrane surface. Interestingly, both cases showed a sudden decrease in O at 6 h, which is the same time that the percentage of C showed a sudden increase.

3.3.3. Sodium (Na), magnesium (Mg), and calcium (Ca)

The percentages of Na in both cases did not significantly change with time. In comparison to Mg and Ca, the concentrations of Na were higher in both feed solutions (SS and SHA); hence, Na had more opportunity to interact with the membrane surface. Therefore, when short-term experiments are considered, Na revealed a greater effect on the fouling formation than Ca and Mg, especially at the early stage of the filtration process; in addition, permeate flux decline is unlikely to be affected by Ca and Mg. Interestingly, the percentages of Na at 2 h of SHAE were much higher than those of SSE. Thus, it is presumed that the organic layer that immediately appeared in the initial stage played an important role in bridging more Na onto the fouled membrane.

3.3.4. Chloride and sulfur

The percentage of chloride (Cl) of SSE increased to 1.85% from its initial value (0%); however, it was independent and did not notably change with operational time. This lack of change is possible because the membrane surface is negatively charged, and hence foulant-membrane electrostatic repulsion occurred due to the double layer and led to a prohibition of Cl deposition on the membrane surface [30]. In contrast, the surface of the SHAE membrane was covered with an organic layer that reduced electrostatic repulsion on membrane surface; thus, it provided more bridging opportunities for Cl on the membrane surface.

The percentages of Sulfur (S) on the fouled membranes from SSE and SHAE decreased from their

Table 4
Chemical compositions of fouling

Time	C		O		F		Na		Mg		S		Cl		K		Ca	
	SS	SHA	SS	SHA	SS	SHA	SS	SHA	SS	SHA	SS	SHA	SS	SHA	SS	SHA	SS	SHA
0	83.04	83.04	14.85	14.85							1.14	1.14						
	(1.74)	(1.74)	(2.05)	(2.05)							(0.21)	(0.21)						
2	76.20	78.69	18.81	22.49	0.69	0.69	2.48	4.97	0.23	0.21	1.77	1.85	2.13	2.13	0.06	0.06	0.08	0.07
	(3.03)	(2.92)	(2.98)	(2.52)	(0.27)	(0.27)	(3.66)	(6.77)	(0.16)	(0.14)	(2.33)	(2.29)	(3.77)	(3.77)	(0.04)	(0.04)	(0.05)	(0.04)
4	68.88	76.13	24.79	30.81	1.62	2.04	2.56	3.97	0.28	0.37	0.69	0.82	1.53	2.56	0.04	0.05	0.03	0.04
	(6.65)	(5.64)	(5.23)	(6.99)	(0.62)	(1.01)	(1.44)	(2.08)	(0.14)	(0.22)	(0.09)	(0.09)	(0.63)	(1.00)	(0.01)	(0.01)	(0.02)	(0.02)
6	75.77	80.26	16.62	20.78	0.41	0.43	3.77	5.78	0.16	0.23	0.76	0.90	2.18	3.34	0.04	0.05	0.06	0.06
	(1.77)	(2.16)	(2.67)	(3.93)	(0.23)	(0.25)	(1.68)	(2.69)	(0.11)	(0.20)	(0.09)	(0.12)	(1.03)	(1.78)	(0.02)	(0.02)	(0.06)	(0.06)
8	75.41	80.47	19.35	23.02	0.77	1.04	3.17	4.19	0.16	0.20	0.84	0.96	1.89	2.49	0.06	0.07	0.05	0.05
	(3.67)	(5.19)	(5.08)	(8.02)	(0.30)	(0.47)	(2.41)	(2.57)	(0.04)	(0.04)	(0.09)	(0.08)	(1.36)	(1.42)	(0.04)	(0.04)	(0.02)	(0.02)
12	71.71	76.35	21.33	24.43	1.55	1.90	3.48	5.32	0.28	0.43	0.75	0.86	2.07	3.12	0.05	0.05	0.04	0.04
	(8.15)	(6.86)	(3.77)	(5.20)	(1.02)	(1.26)	(2.13)	(3.93)	(0.17)	(0.22)	(0.11)	(0.12)	(1.36)	(2.40)	(0.02)	(0.02)	(0.01)	(0.02)
20	69.44	75.84	23.61	28.78	1.41	1.89	2.99	4.16	0.19	0.27	0.70	0.84	1.85	2.53	0.03	0.04	0.06	0.06
	(6.97)	(4.34)	(5.23)	(8.07)	(0.60)	(1.04)	(1.05)	(1.34)	(0.11)	(0.18)	(0.21)	(0.28)	(0.63)	(0.82)	(0.01)	(0.03)	(0.02)	(0.03)

Note: Values inside parentheses indicate the standard deviation of the chemical compositions of fouling.

initial value (1.14%) to 0.70 and 0.84%, respectively. However, as the fouling layer increasingly covered the membrane surface, the portion of S detected gradually decreased. Interestingly, the percentage of S in SHAE was more than for SSE, especially at the initial stage. This difference indicates that the source of S is most likely SO_4^{2-} from the feed solution as the SO_4^{2-} is the only S source in the feed solution (Table 1).

According to the results of inorganic ion particles, it is possible that fouling mechanism of ions may take place by crystallization or particles fouling [31]. Crystallization can occur according to precipitation of ions; while particles fouling can happen due to the accumulation of particles onto membrane surface and then forming cake layer [32]. However, more experiments are required to examine the dominant mechanism during SWRO process.

4. Conclusion

In this study, TSFEs were conducted in order to investigate the effect of humic acid on the fouling mechanism of SWRO, based on the use of two feed solutions: SS and SHA. Time-series image analysis (TSIAs) were then applied to evaluate the fouling mechanisms of the SWRO process. The results revealed that humic acid in the SHA solution affected the SWRO process by causing a severe decline in the membrane performance. A full formation of the organic layer in the first 2 h was observed when humic acid was added to the feed solution. The organic layer was possible to interact with charged inorganic particles. This interaction could be confirmed by the higher percentage of elements (e.g. O, Na, Cl, and F) on the surface of the fouled SHAE membrane. On the other hand, at 20 h of SSE, the membrane surface was partially covered by inorganic particles, causing a lower flux decline than for SHAE.

Based on the TSIA results, it could be clearly verified that the surface morphologies of SHAE and SSE were different. The fouling mechanism of SSE can be described by the deposition of inorganic particles on the membrane. In SHAE, the fouling mechanism is based on the adsorption of humic substances and the deposition of other inorganic foulants onto the membrane surface. The subsequent results of AFM and SEM analyses support the fact that development of the organic layer occurred at an early stage of SHAE, leading the membrane surface to become smoother compared to SSE.

Acknowledgments

This research was supported by a grant (07seahero B02-01) from the Plant Technology Advancement Program funded by the Ministry of Land, Transport and Maritime Affairs of the Korean government. We also thank Woongjin Chemical Co., Suwon 443-270, South Korea for supporting RO membranes.

References

[1] M.R. Al-Agha, R.S. Mortaja, Desalination in the Gaza strip: Drinking water supply and environmental impact, Desalination 173 (2005) 157–171.
[2] B. Nicolaisen, Developments in membrane technology for water treatment, Desalination 153 (2002) 355–360.
[3] M.A. Rvias, R. Paley, Drinking water from the sea, World Pumps 475 (2006) 56–58.
[4] Y.M. Kim, Kim, S. J., Kim, Y. S., Lee, S., Kim, I. S., Kim, J. H., Overview of systems engineering approaches for large scale seawater desalination plant with reverse osmosis network., Desalination 238 (2009) 312–332.
[5] Y.G. Lee, Y.S. Lee, J.J. Jeon, S. Lee, D.R. Yang, I.S. Kim, J.H. Kim, Artificial neural network model for optimizing operation of a seawater reverse osmosis desalination plant, Desalination 249 (2009) 180–189.
[6] S.J. Kim, Y.G. Lee, K.H. Cho, Y.M. Kim, S. Choi, I.S. Kim, D.R. Yang, J.H. Kim, Site-specific raw seawater quality impact study on SWRO process for optimizing operation of the pressurized step, Desalination 238 (2009) 140–157.
[7] S.J. Kim, Y.G. Lee, S. Oh, Y.S. Lee, Y.M. Kim, M.G. Jeon, S. Lee, I.S. Kim, J.H. Kim, Energy saving methodology for the SWRO desalination process: Control of operating temperature and pressure, Desalination 249 (2009) 260–270.
[8] S.J. Kim, S. Oh, Y.G. Lee, M.G. Jeon, I.S. Kim, J.H. Kim, A control methodology for the feed water temperature to optimize SWRO desalination process using genetic programming, Desalination 249 (2009) 190–199.
[9] K. Burashid, A.R. Hussain, R.O. Seawater, Plants: Operation and maintenance experience: Addur desalination plant operation assessment, Desalination 165 (2004) 11–22.
[10] A.G.I. Dalvi, R. Al-Rasheed, M.A. Javeed, Studies on organic foulants in the seawater feed of reverse osmosis plants of SWCC, Desalination 132 (2000) 217–232.
[11] S.S. Sablani, M.F.A. Goosen, R. Al-Belushi, M. Wilf, Concentration polarization in ultrafiltration and reverse osmosis: A critical review, Desalination 141 (2001) 269–289.
[12] D. Kim, S. Jung, J. Sohn, H. Kim, S. Lee, Biocide application for controlling biofouling of SWRO membranes—an overview, Desalination, 238 (2009) 43–52.
[13] T. Tran, B. Bolto, S. Gray, M. Hoang, E. Ostarcevic, An autopsy study of a fouled reverse osmosis membrane element used in a brackish water treatment plant, Water Res. 41 (2007) 3915–3923.
[14] M. Moonkhum, Y.G. Lee, Y.S. Lee, J.H. Kim, Review of seawater natural organic matter fouling and reverse osmosis transport modeling for seawater reverse osmosis desalination, Desalin. Water Treat. 15 (2010) 92–107.
[15] S. Lee, J.-S. Choi, C.-H. Lee, Behaviors of dissolved organic matter in membrane desalination, Desalination 238 (2009) 109–116.
[16] S. Lee, S. Kim, J. Cho, E.M.V. Hoek, Natural organic matter fouling due to foulant-membrane physicochemical interactions, Desalination 202 (2007) 377–384.
[17] B.K.N. Park, S.-D. Kim, J. Cho, Characterizations of the colloidal and microbial organic matters with respect to membrane foulants, J. Membr. Sci. 275 (2006) 29–36.
[18] J. Cho, G. Amy, J. Pellegrino, Membrane filtration of natural organic matter: Comparison of flux decline, NOM rejection, and foulants during filtration with three UF membranes, Desalination 127 (2000) 283–298.
[19] R.P. Schneider, L.M. Ferreira, P. Binder, J.R. Ramos, Analysis of foulant layer in all elements of an RO train, J. Membr. Sci., 261 (2005) 156–162.
[20] M. Herzberg, M. Elimelech, Biofouling of reverse osmosis membranes: Role of biofilm-enhanced osmotic pressure, J. Membr. Sci. 295 (2007) 11–20.
[21] H.K. Shon, S. Vigneswaran, In S. Kim, J. Cho, H.H. Ngo, Effect of pretreatment on the fouling of membranes: Application in biologically treated sewage effluent, J. Membr. Sci. 234 (2004) 111–120.
[22] T.C.J.E. Drewes, C. Higgins, P. Xu, Membrane characterization and autopsy and water quality analysis: Analytical capabilities and techniques, Report of Advanced Water Technology Center (AQWATEC), Colorado School of Mines (CSM), Environmental Science & Engineering Division Golden, CO 80401–1887, (2010).
[23] M. Pontié, S. Rapenne, A. Thekkedath, J. Duchesne, V. Jacquemet, J. Leparc, H. Suty, Tools for membrane autopsies and antifouling strategies in seawater feeds: A review, Desalination 181 (2005) 75–90.
[24] V.L.W. Gene V Glass, John Mordechai Gottman, Design and Analysis of Time-Series Experiments, Information Age, Charlotte, NC, ISBN-978-1-59311-980-5 (2008).
[25] B. Tansel, J. Sager, J. Garland, S. Xu, Effect of transmembrane pressure on overall membrane resistance during cross-flow filtration of solutions with high-ionic content, J Memb Sci. 328 (2009) 205–210.
[26] B. Mi, M. Elimelech, Organic fouling of forward osmosis membranes: Fouling reversibility and cleaning without chemical reagents, Journal of Membrane Science 348 (2010) 337–345.
[27] M.E.a.A.E. Childres, Zeta potential of—reverse osmosis membranes: Impllcatlons for membrane performance, Water Treatment Technology Program Report No. 10, (1996).
[28] S. Lee, M. Elimelech, Relating organic fouling of reverse osmosis membranes to intermolecular adhesion forces, Environ. Sci. Technol. 40 (2006) 980–987.
[29] A.W. Zularisam, A.F. Ismail, R. Salim, Behaviours of natural organic matter in membrane filtration for surface water treatment—a review, Desalination 194 (2006) 211–231.
[30] A.E.C.a.M. Elimelech, Relating nanofiltration membrane performance to membrane charge (electrokinetic) characteristics, Environ. Sci. Technol. 34 (2000) 3710–3716.
[31] R. Sheikholeslami, Calcium sulfate fouling-precipitation or particulate: A proposed composite model, Heat Transfer Engineering 21 (2000) 24–33.
[32] M.E.X. Zhu, Colloidal fouling of reverse osmosis membranes: Measurements and fouling mechanisms, Environ. Sci. Technol. 31 (1997) 3654–3662.